RSC Applied Polymers

Accepted Manuscript

This article can be cited before page numbers have been issued, to do this please use: M. Wei, Y. Yao, Y. Liu, M. P. H. Pedige, X. Li, Y. Hsu, H. Uyama, W. Lu and T. Chen, *RSC Appl. Polym.*, 2026, DOI: 10.1039/D6LP00162A.

ROYAL SOCIETY OF CHEMISTRY

rsc.li/RSCApplPolym

View Article Online
DOI: 10.1039/D6LP00162A

ARTICLE

Dual-crosslinked poly(γ-glutamic acid)/chitosan nanofiber composite films with enhanced wet mechanical stability

Received 00th January 20xx,
Accepted 00th January 20xx

DOI: 10.1039/x0xx00000x

Meng Wei,[†a] Ying Yao,[†b] Yingbu Liu,[†b] Madhurangika Panchabashini Horathal Pedige,[b] Xuke Li,[a] Yu-I Hsu,[*b] Hiroshi Uyama,[*b] Wei Lu,[*a] Tao Chen[*a]

Poly(γ-glutamic acid) (PGA) is a biodegradable microbial polypeptide with potential for sustainable film materials, but its strong hydrophilicity and swelling tendency limit its mechanical stability under wet conditions. Herein, we report dual-crosslinked PGA/chitosan nanofiber (CsF) composite films with improved water resistance, enhanced wet mechanical stability, and tunable degradability. PGA was modified with furan groups and covalently crosslinked with 4-arm poly(ethylene glycol) maleimide through a Diels–Alder reaction, while CsF served as a physical crosslinking domain through electrostatic interactions between its amino groups and the carboxyl groups of PGA. Notably, as the CsF content increased from 0 to 1.0 wt%, the mechanical strength of the composite films markedly improved. The optimized 1.0 wt% CsF film showed a dry tensile strength of 75.7 MPa, 8.7 times higher than that of the neat film, and retained a wet tensile strength of 4.3 MPa and a wet toughness of 1.12 MJ m^{-3} in the fully swollen state in deionized water. This wet-state robustness was further supported by a reduced equilibrium swelling ratio of 951% and an increased water contact angle from 25° to 85°. Moreover, the films exhibited complete degradation within 60 days in natural soil and 90 days in enzyme-containing artificial seawater. This work provides a feasible strategy for balancing wet mechanical robustness and degradability in PGA-based sustainable films.

Introduction

The persistent accumulation of petroleum-derived plastic waste in natural ecosystems has become a global environmental concern because of its non-renewable origin and poor degradability under natural conditions.[1–3] To mitigate this problem, biodegradable polymer films derived from renewable resources have attracted increasing attention as sustainable alternatives to conventional plastics, offering useful performance during use and improved environmental compatibility after disposal.[4–7]

Natural polymers, especially polysaccharides and proteins/polypeptides, have been widely investigated as renewable raw materials for biodegradable plastic films.[8–11] Among them, poly(γ-glutamic acid) (PGA) is a naturally occurring anionic polypeptide produced by microbial fermentation, particularly by Bacillus subtilis.[12–14] PGA consists of glutamic acid units linked through amide bonds between the α-amino and γ-carboxyl groups, resulting in a water-soluble polypeptide with high biocompatibility, low toxicity, and biodegradability.[15,16] The abundant carboxyl groups along the PGA backbone enable electrostatic interactions with oppositely charged polymers, providing a simple route for constructing PGA-based assemblies. Based on this feature, multilayer assembly between PGA and amino-functional biopolymers, such as poly(L-lysine) and chitosan, has been widely used to prepare PGA-based films.[17,18] However, these layer-by-layer assembled films are mainly stabilized by physical electrostatic interactions. As a result, their mechanical strength and dimensional stability are often insufficient for practical applications.

To overcome these limitations, several strategies have been developed, including chemical crosslinking and physical blending with hydrophobic polymer components.[19–23] For instance, Weepol et al.[20] prepared robust PGA composite films by in situ methylation of PGA using H_2SO_4 followed by blending with poly(lactic acid), achieving a tensile strength of 24.55 MPa. Yao et al.[21] modified PGA with hydrazide groups and subsequently reacted it with acetoacetylated poly(vinyl alcohol) to fabricate PGA composite films through dynamic Schiff-base crosslinking. The resulting films exhibited excellent dry mechanical performance, with a tensile strength of 123.5 MPa. These studies show that chemical crosslinking and hydrophobic polymer blending can effectively strengthen PGA-based films. However, the abundant carboxyl groups in PGA still make these films vulnerable to water uptake, swelling, and

[a] State Key Laboratory of Advanced Marine Materials, Zhejiang Key Laboratory of Extreme-environmental Material Surfaces and Interfaces, Ningbo Institute of Materials Technology and Engineering, Chinese Academy of Sciences, Ningbo 315201, China.
[b] Department of Applied Chemistry, Graduate School of Engineering, Osaka University, 2-1 Yamadaoka, Suita, Osaka 565-0871, Japan.
† These authors contributed equally to this work.
Electronic Supplementary Information (ESI) available.

View Article Online
DOI: 10.1039/D6LP00162A

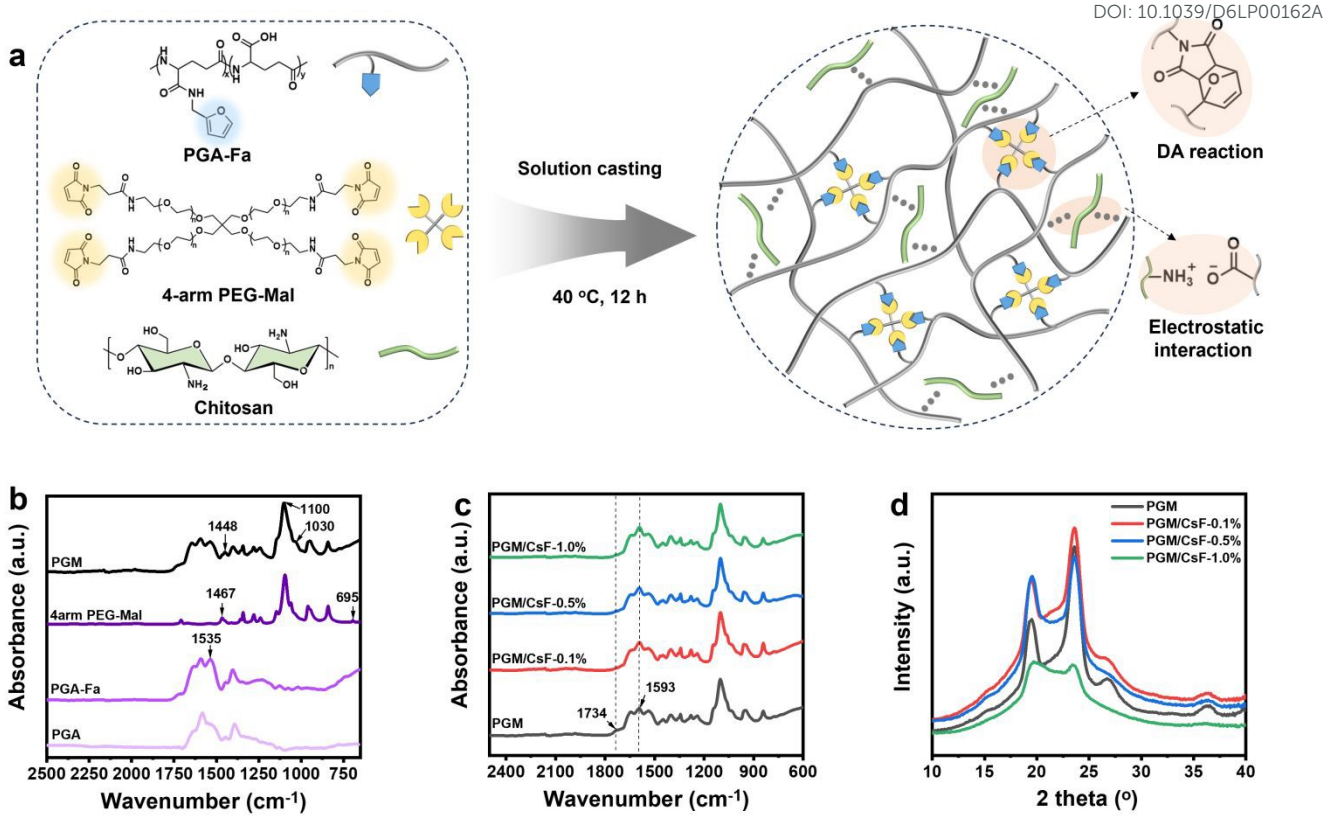

Fig.1 (a) Schematic illustration of PGM/CsF films. (b) FTIR of PGA, PGA-Fa, 4arm PEG-Mal and neat PGM film. (c) FTIR of PGM/CsF films with different CsF content. (d) WAXS of neat PGM and PGM/CsF films.

structural instability in aqueous environments. In addition, although the incorporation of hydrophobic polymers can improve water resistance, it often slows the degradation of PGA-based films. Therefore, it remains challenging to develop PGA-based sustainable films with suppressed swelling, wet mechanical stability, and controllable degradability.

Herein, we report a PGA-based composite film with improved wet-state stability and retained degradability. This design addresses a key limitation of highly hydrophilic PGA films, where abundant carboxyl groups provide ionic interaction sites but also cause severe water uptake and wet-state mechanical weakening. PGA was first modified with furan groups and covalently crosslinked with 4-arm poly(ethylene glycol) maleimide (4-arm PEG-Mal) through a Diels–Alder (DA) reaction to construct a stable primary network. Chitosan nanofibers (CsF) were further introduced as multifunctional reinforcing and ionic-crosslinking domains through electrostatic interactions with PGA. In this design, CsF not only reinforces the film mechanically but also regulates swelling by forming a bio-based polypeptide/polysaccharide network. Unlike PGA films based solely on electrostatic assembly, chemical crosslinking, or hydrophobic blending, the present system combines structural integrity, wet-state reinforcement, swelling suppression, and retained degradability within one bio-based film platform. This work provides a feasible strategy for developing bio-based polypeptide/polysaccharide composite films that combine wet-state mechanical robustness with environmentally relevant degradability.

Results and discussion

Fabrication and characterization of PGM/CsF films

PGA was first modified with furfurylamine to introduce furan groups, yielding furan-modified PGA (PGA-Fa) (**Fig. S1**). The degree of substitution was determined to be approximately 7% based on ^{1}H NMR analysis (**Fig. S2**). The film prepared from PGA-Fa and 4-arm PEG-Mal was named PGM. Subsequently, PGM/CsF composite films were fabricated by incorporating CsF into the PGM matrix, as schematically illustrated in **Fig. 1a**. The morphology of the CsF was characterized by SEM, as shown in **Fig. S3**. The CsF exhibited an entangled fibrillar morphology, and the average fiber diameter was approximately 160 nm, as determined using ImageJ analysis. The successful occurrence of the Diels–Alder (DA) reaction was confirmed by FT-IR spectroscopy (**Fig. 1b**). The characteristic peaks of the maleimide ring in 4-arm PEG-Mal, observed at 1467 cm^{-1} (C–N–C stretching) and 695 cm^{-1} (C=C–H out-of-plane bending), completely disappeared in the PGM spectrum. Concurrently, a new peak emerged at 1448 cm^{-1}, which is attributed to the vibration of the newly formed DA adduct. Moreover, the intense absorption bands at 1100 cm^{-1} and 1030 cm^{-1}

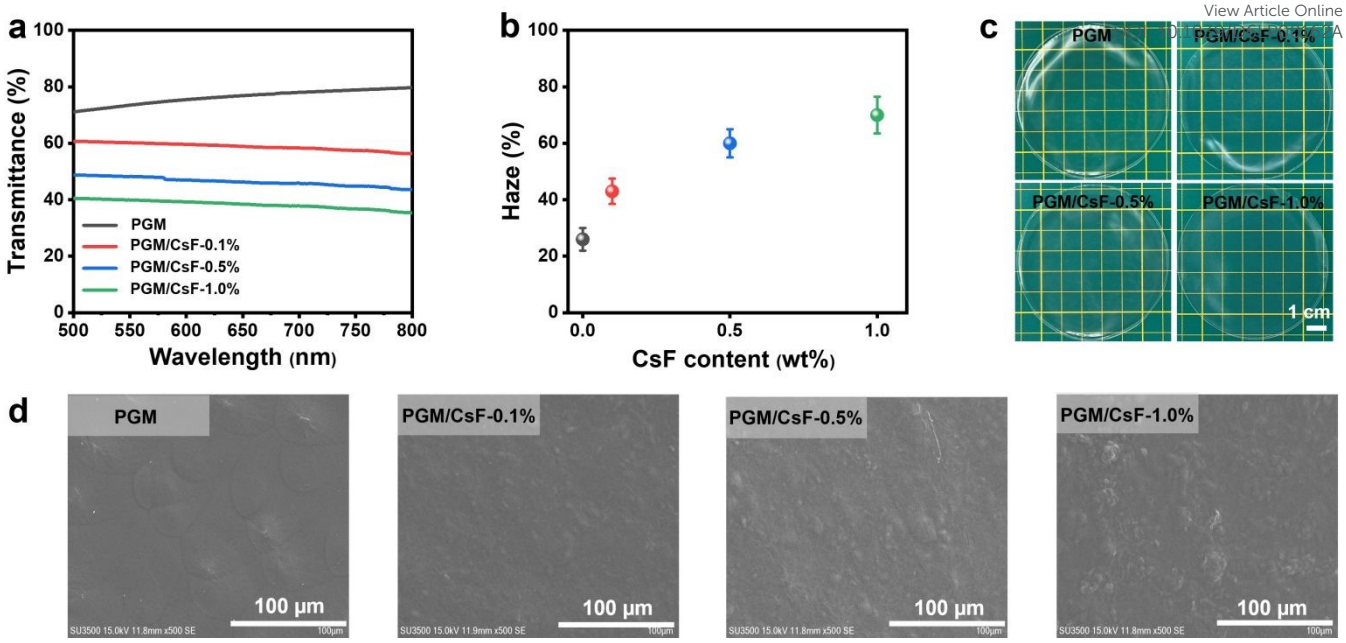

Fig.2 (a)Transmittance, (b) haze, (c) appearance, and (d) surface morphologies of neat PGM and PGM/CsF films.

in the PGM spectrum, corresponding to the C–O–C stretching of the PEG backbone, further verify the successful integration of the PEG cross-linker in the polymer network. The secondary non-covalent interactions introduced by CsF are evidenced in **Fig. 1c**. In the neat PGM film, a distinct peak at 1734 cm^{-1} corresponding to the stretching vibration of free –COOH groups was observed. However, upon the addition of CsF, this peak significantly diminished, while the symmetric stretching of carboxylate groups ($–COO^-$) at 1593 cm^{-1} intensified with increasing CsF content. This transition confirms the occurrence of proton transfer and the formation of robust electrostatic interactions between the carboxyl groups of PGA-Fa and the amino groups of CsF. Furthermore, the crystalline structure of the composite films was investigated by WAXS (**Fig. 1d**). The neat PGM film exhibited sharp diffraction peaks at 19.5°, 23.7°, 26.8°, and 36.4°, which are characteristic of PEG crystallization. With the increasing CsF content, these peaks became noticeably broader, a trend consistent with the 2D WAXS patterns (**Fig. S4**). The relative crystallinity of PEG domains decreased from 40.2% for neat PGM to 39.8%, 32.5%, and 21.4% for PGM/CsF-0.1%, PGM/CsF-0.5%, and PGM/CsF-1.0%, respectively, indicating that CsF restricts PEG chain packing and reduces the crystalline order of PEG domains. These results collectively confirm the successful fabrication of PGM/CsF composite films by DA reaction and electrostatic interaction.

Optical Transparency and Haze of PGM/CsF films

Optical transparency is an important parameter for biodegradable wrapping and protective film applications, where visual inspection of the covered materials is often required. The transmittance of the PGM/CsF composite films in the visible range (500–800 nm) are presented in **Fig. 2a**. The neat PGM film exhibited a high transmittance of approximately 79.8% at 600 nm, indicating its good inherent clarity. Upon the incorporation of CsF, the transmittance of the composite films gradually decreased, reaching a minimum of 40.1% for the PGM/CsF-1.0% sample. Correspondingly, the haze increased from approximately 26% for neat PGM to 70% for PGM/CsF-1.0% (**Fig. 2b**). The visual appearance of the films, as displayed in **Fig. 2c**, is consistent with these optical results. Despite the decrease in transmittance, all composite films retained sufficient clarity to be observed, suggesting their suitability for applications requiring moderate transparency rather than high optical clarity, such as biodegradable wrapping films, semi-transparent protective layers, or short-term covering/protective films. In these scenarios, a balance between mechanical stability and acceptable transparency is more important than maximum optical clarity. The reduction in transparency and the concomitant increase in haze can be attributed to the light scattering caused by the introduced chitosan nanofibers. This is further supported by the surface morphologies observed via SEM (**Fig. 2d**). While the neat PGM film presented a relatively smooth surface, the PGM/CsF films exhibited increased surface roughness with visible micro-scale textures. This structural transition indicates the successful integration of CsF within the PGA matrix, where the CsF induce surface irregularities.

Dry-state mechanical performance of PGM/CsF films

The mechanical performance of the PGM/CsF composite films in the dry state, including tensile strength and rheological behavior, was systematically investigated. As a control, PGA/CsF-1.0% was prepared from PGA and CsF without 4-arm PEG-Mal. The film was too brittle and could not provide valid tensile results. The neat PGM film exhibited a relatively low tensile strength of 8.7 MPa and an elongation at break of 10.6% (**Fig. 3a–c**). For the PGM/CsF-1.0% film, the tensile strength enhanced to 75.7 MPa, representing an approximately 8.7-fold increase compared to the neat PGM

View Article Online
DOI: 10.1039/D6LP00162A

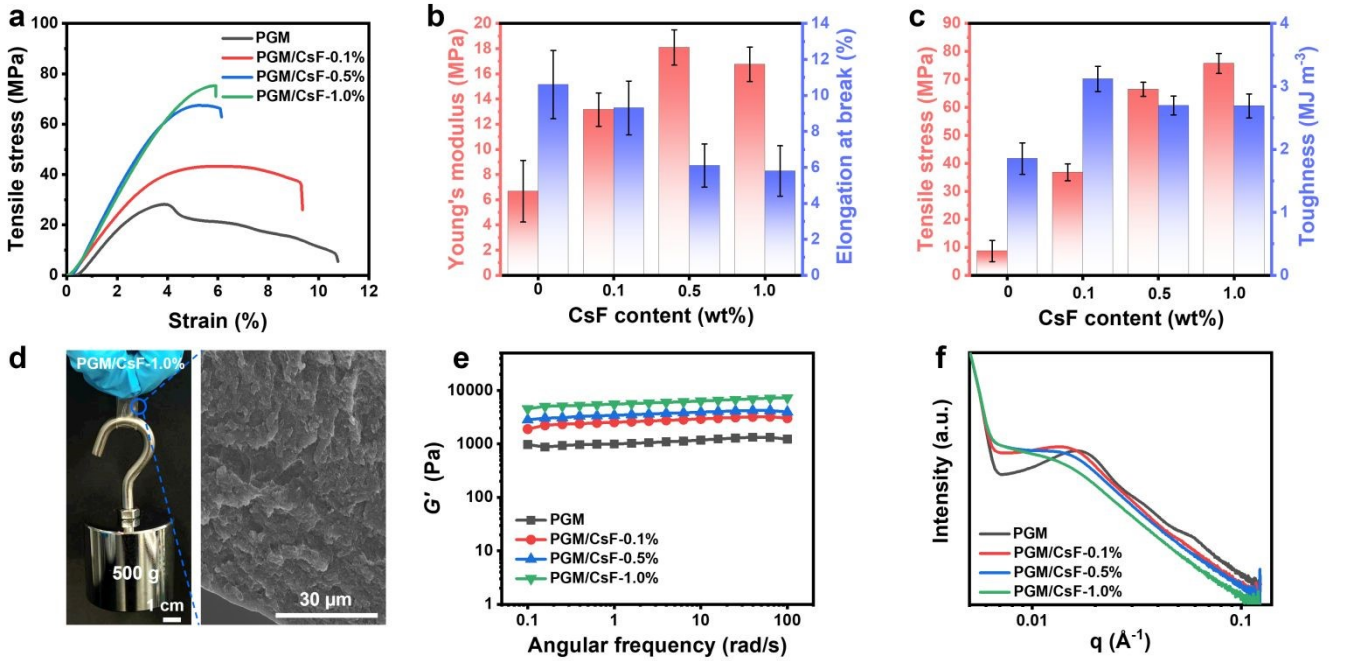

Fig.3 (a) Tensile stress-strain curves of neat PGM and PGM/CsF films. (b, c) Comparison of Young's modulus, elongation at break, tensile strength, and toughness. (d) Image of a PGM/CsF-1.0% film supporting a 500 g weight and the corresponding cross-sectional SEM image. (e) G' of PGM and PGM/CsF films. (f) SAXS profiles of neat PGM and PGM/CsF films.

(**Fig. 3a–c**). Concurrently, the Young's modulus increased from 6.7 MPa to 16.8 MPa, and the toughness increased from 1.85 MJ m^{-3} to 2.69 MJ m^{-3} (**Fig. 3a–c**). Although the elongation at break decreased to 5.8%, the overall mechanical robustness was remarkably improved. This was demonstrated by the PGM/CsF-1.0% film successfully supporting a 500 g weight (**Fig. 3d**). Compared with neat PGM, the PGM/CsF films showed nanofiber-containing cross-sectional morphologies (**Fig. 3d** and **Fig. S5**), confirming the incorporation of CsF as reinforcing domains within the PGM matrix. TGA results further showed that the thermal stability of the films was largely retained after CsF incorporation (**Fig. S6**). To clarify the origin of this mechanical reinforcement, rheological and gel fraction analyses were further performed. As shown in **Fig. 3e** and **Fig. S7**, the storage modulus (*G'*) of PGM was 997 Pa, which was higher than that of PGA/CsF-1.0% (313 Pa). This indicates that the PGA/CsF electrostatic network alone was insufficient for mechanical stability and confirms the contribution of the DA covalent network. With the incorporation of 1.0 wt% CsF, the *G'* of the PGM/CsF film further increased to 5556 Pa (**Fig. 3e**), suggesting that CsF introduced additional electrostatic crosslinking points and strengthened the dual-crosslinked network. The gel fraction also increased from 69.9% for neat PGM to 90.7% for PGM/CsF-1.0% (**Fig. S8**). This result further supports the formation of a denser network structure. DMA analysis showed broadened and intensified tanδ peaks after CsF incorporation (**Fig. S9**), indicating more pronounced viscoelastic relaxation and enhanced energy dissipation in the composite network. DSC analysis showed decreased melting enthalpy at 40–50 °C (**Fig. S10**), suggesting disturbed PEG chain packing. These results imply that the reinforcement mainly originated from the dual-crosslinked network rather than increased PEG crystallinity. To further investigate the mesoscopic structure of the films, SAXS analysis was performed (**Fig. 3f**). The SAXS profile of the neat PGM film displayed a distinct scattering peak, corresponding to a characteristic distance of 37.0 nm, which is attributed to the periodic organization of PEG-rich domains within the DA-crosslinked network. The characteristic distance increased to 41.1, 42.7, and 46.5 nm with increasing CsF content, accompanied by a weakened and broadened scattering peak. These results, together with the decreased PEG crystallinity observed in WAXS and DSC, indicate that CsF disrupted PEG chain ordering. Therefore, the enhanced mechanical strength mainly originated from the denser dual-crosslinked network formed by DA covalent bonds and PGA-Fa/CsF electrostatic interactions.

Wet-state mechanical stability of PGM/CsF films

The tensile properties of the PGM/CsF films in the wet state are illustrated in **Fig. 4a–c**. The neat PGM film was tested after 30 s of water immersion before disintegration, while the PGM/CsF films were tested after reaching the swollen state. The neat PGM film exhibited a tensile strength of 0.4 MPa and a low elongation at break. In stark contrast, the incorporation of CsF significantly enhanced the wet mechanical performance. For the PGM/CsF-1.0% film, the wet tensile strength reached 4.3 MPa, and the elongation at break surged to approximately 50%, a 10-fold improvement from the 5.8% observed in the

View Article Online
DOI: 10.1039/D6LP00162A

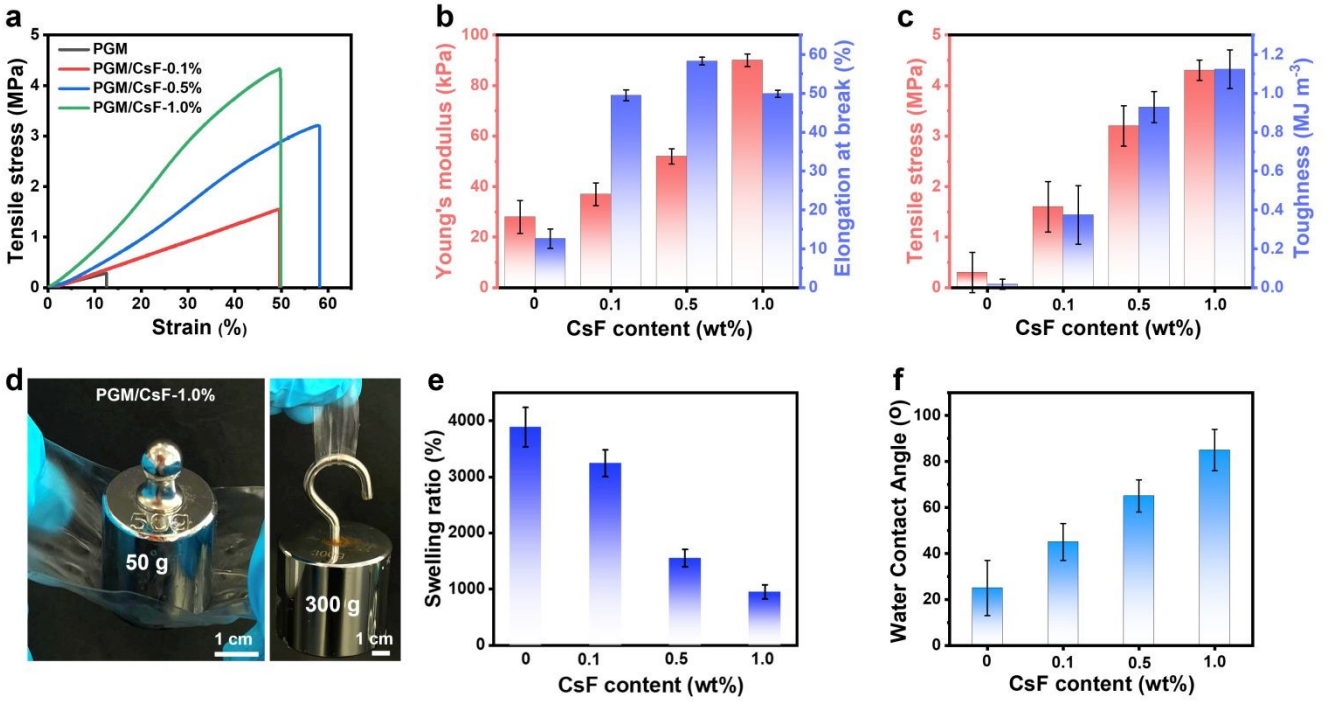

Fig.4 (a) Tensile stress-strain curves of neat PGM and PGM/CsF films. (b, c) Comparison of Young's modulus, elongation at break, tensile strength, and toughness. (d) Image of a swollen PGM/CsF-1.0% film supporting a 50 g and 300 g weight. (e, f) Swelling ratio and water contact angle of neat PGM and PGM/CsF films. (The wet-state mechanical strength and swelling ratio of neat PGM were measured after 30 s of water immersion before disintegration.)

dry state. Notably, the wet Young's modulus and toughness of the PGM/CsF-1.0% film were 90 kPa and 1.12 MJ m^{-3}, respectively, marking a 3.0-fold and 62-fold increase compared to those of the neat PGM. This remarkable wet-state stability of PGM/CsF-1.0% film is demonstrated in **Fig. 4d**, where the swollen film could easily support a 50 g weight and withstand a 300 g load without fracture. The improved wet mechanical stability is closely related to the suppressed swelling behavior of the PGM/CsF films. As illustrated in **Fig. 4e** and **Fig. S11**, the neat PGM film disintegrated after 1 min of immersion. In contrast, the PGM/CsF films maintained their structural integrity, with the equilibrium swelling ratio decreasing dramatically from 3247% (PGM/CsF-0.1%) to 951% (PGM/CsF-1.0%) as the CsF content increased. This trend suggests that the rigid CsF nanofibers, coupled with robust electrostatic cross-linking, facilitate the formation of a highly dense internal network. This is further corroborated by the water contact angle (WCA) measurements (**Fig. 4f**), where the WCA increased from 25° to 85° upon CsF addition. As discussed above, CsF incorporation led to a higher gel fraction (**Fig. S8**) and a rougher surface (**Fig. 2d**), which suppress water penetration and increase the water contact angle (**Fig. S12**). Therefore, the improved WCA reflects enhanced apparent water resistance of the composite films. Collectively, these results show that the dual-network strategy suppresses over-hydration of PGA chains. The DA covalent bonds maintain structural integrity, while the PGA-Fa/CsF electrostatic interactions provide additional physical crosslinking points and stabilize the films in the swollen state. The PGM/CsF-1.0% film showed the best overall balance among mechanical reinforcement, wet-state stability, swelling resistance, and acceptable visual transparency. Therefore, PGM/CsF-1.0% was selected as the optimized composition. In the wet state, PGM/CsF-1.0% could be bent and twisted (**Fig.S13**), demonstrating good flexibility. Importantly, the film could support a 300 g load underwater (**Fig.S14**). Furthermore, PGM/CsF-1.0% maintained stable *G'* after storage at room temperature and 40% RH for 10 days (**Fig. S15**). In the swollen state, the rheological results showed that *G'* of PGM/CsF-1.0% remained stable for 5 days and decreased after 7 days (**Fig. S16**). After 10 days of immersion, the film ruptured, resulting in a marked decrease in *G'* (**Fig. S16**), indicating short-term underwater mechanical stability.

Degradation behavior of PGM/CsF films

Considering the increasing interest in mechanically robust yet degradable bio-based films, the degradation behavior of the PGM/CsF films was further investigated.[24] The environmental degradability of PGM/CsF films was systematically evaluated by monitoring mass variations over time in both natural soil and artificial seawater (ASW) (**Fig. 5**). In the soil environment (**Fig. 5a**), the neat PGM film underwent complete decomposition within 40 days. With the incorporation of 1.0 wt% CsF, the degradation period was extended to 60 days. The observed decrease in degradation rate with higher CsF loading is primarily attributed to the increased density of electrostatic interactions within the dual-network. Considering the increasing attention paid to seawater-degradable plastics, the

View Article Online
DOI: 10.1039/D6LP00162A

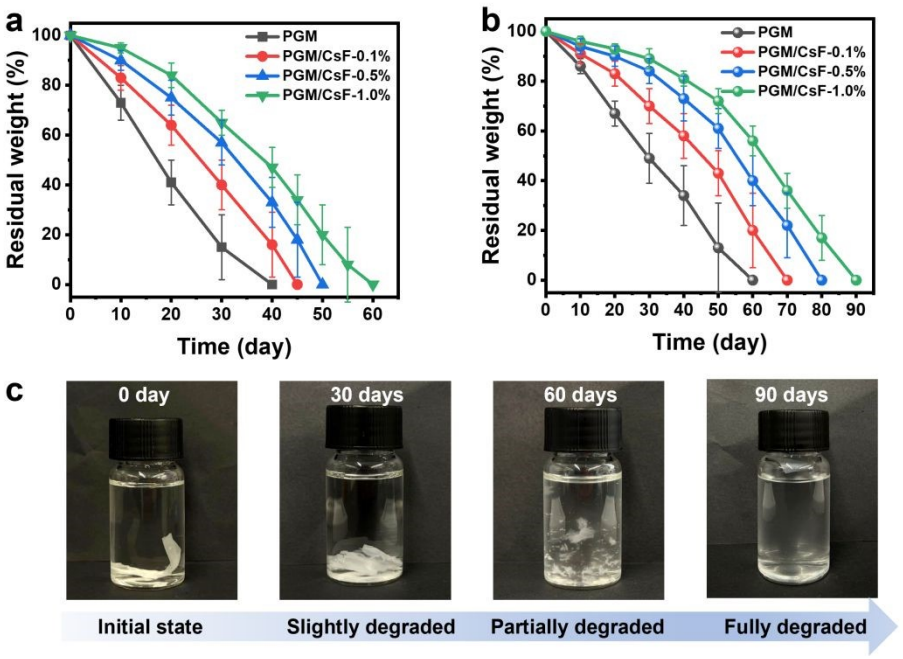

Fig.5 Degradation and disintegration of the neat PGM and PGM/CsF films. (a) Residual weight of the neat PGM and PGM/CsF films as a function of time in the soil (City of Ningbo). (b) Residual weight of the neat PGM and PGM/CsF films as a function of time in in artificial seawater (ASW) containing γ-glutamyl transpeptidase (10 U/mL) (c) Image of a PGM/CsF-1.0% film after it was immersed in ASW.

degradation behavior of the films in ASW was further investigated.[25,26] As shown in **Fig. S17**, the equilibrium swelling ratios in ASW were recorded at 640%, 633%, 523%, and 498% for films containing 0, 0.1%, 0.5%, and 1.0% CsF, respectively. The lower swelling ratio in ASW than in pure water is likely due to the charge-screening effect of saline ions. A similar degradation trend was observed in the marine-simulated environment (**Fig. 5b**), although the overall rates were notably slower than those in soil. For instance, the PGM/CsF-1.0% film exhibited a prolonged degradation period of approximately 90 days in ASW, whereas the neat PGM film underwent total mass loss within 60 days. The visual evolution of the films during ASW immersion is captured in **Fig. 5c**. The PGM/CsF-1.0% film maintained its structural integrity during the initial 30 days, followed by significant fragmentation by Day 60, and finally transitioned into a fully degraded state by Day 90. The degradation of PGM/CsF films is mainly caused by water penetration, PGA chain swelling, and gradual network loosening. Microorganisms and enzymes in soil and enzyme-containing artificial seawater further promote chain scission of PGA and CsF segments. These processes lead to weight loss and the release of water-soluble fragments.[27-29] The difference between soil and marine degradation rates likely stems from the significantly higher microbial density and enzymatic activity present in natural soil compared to the ASW medium. Taken together, the dual-crosslinked PGM/CsF films showed a favorable balance of mechanical robustness, wet-state stability, and tunable degradation compared with representative biodegradable polymer films, including PGA-, chitosan-, starch-, and poly(lactic acid)-based films (**Table S1**). This balance highlights their potential as biodegradable film materials.

Experimental

Materials

Poly(γ-glutamic acid) (PGA, M_w=1.6×10^5 g/mol) was provided by Kookmin University (Seoul, Korea). Furfurylamine (Fa) was purchased from Wako Chemicals (Osaka, Japan). 1-(3-Dimethylaminopropyl)-3-ethylcarbodiimide hydrochloride (EDC) and N-hydroxysuccinimide (NHS) were purchased from Tokyo Chemical Industry (Tokyo, Japan). 2-Morpholinoethanesulfonic acid (MES), γ-glutamyl transpeptidase and sodium azide were purchased from Sigma-Aldrich (St. Louis, MO). 4-arm poly(ethylene glycol) maleimide (4-arm PEG-Mal, M_w = 5.0 × 10^3 g/mol) was purchased from PolyScience (PA, USA). Chitosan nanofiber (CsF, derived from crab shell) was obtained from Sugino Machine Limited (Japan). Artificial seawater (ASW) solution was made using Daigo's Artificial Seawater SP for Marine Microalgae Medium from Shiotani MS Corporation, Japan. All reagents were used without further purification.

Synthesis of PGA–Fa

PGA (1.3 g, 10 mmol) was dissolved in 130 mL of MES buffer (0.1 mol/L, pH 5.5), Subsequently, the carboxylic groups were activated by adding EDC (1.9 g, 10 mmol), and NHS (1.2 g, 10 mmol) for 30 min. Then, Fa (0.29 g, 2.0 mmol) was added to this solution, and stirring of the mixture was conducted for 24 h at 25 °C. The reaction solution was subjected to dialysis against 0.1mol/L NaCl solution for 2 days then deionized water for 4 days using a dialysis membrane with a MWCO of 1 × 10^4.

Thereafter, a white spongy PGA-Fa product was obtained by lyophilization.

The structure of PGA-Fa was confirmed using ^{1}H NMR: ^{1}H NMR (400 Hz, D_2O, ppm) δ: 1.82(d, 2H, $-CH_2-$), 2.19 (s, 2H, $-COCH_2-$), 4.01 (t, H, α-CH−), 4.32 (t, H, α-CH−), 6.09 (s, H, $-C_4HC-$),6.43 (s, H, $-C_4H-$), 7.25 (s, H, $-C_4HO-$).

Preparation of PGM/CsF films

The composite films were fabricated via a solution casting. Briefly, 1.0 g of PGA-Fa was dissolved in 10 mL of deionized water to form a clear solution. To this, 0.65 g of 4-arm PEG-Mal was added to maintain a stoichiometric 1:1 molar ratio of furan to maleimide groups. After thorough magnetic stirring, various amounts of CsF were incorporated into the mixture to achieve final concentrations of 0, 0.1, 0.5, and 1.0 wt%. The resulting mixtures were cast into Petri dishes, and reacted at 40 °C for 12 h to ensure complete cross-linking. The obtained films were designated as PGM (neat film), PGM/CsF-0.1%, PGM/CsF-0.5%, and PGM/CsF-1.0%, respectively. As a control, PGA/CsF-1.0% was prepared by directly incorporating 1.0 wt% CsF into the PGA solution without adding 4-arm PEG-Mal, with all other preparation conditions kept consistent.

Conclusions

In summary, we developed a robust bio-based PGM/CsF composite film by integrating a covalent DA network with electrostatic interactions. The covalent network provided structural integrity, while the electrostatic interactions between PGA and CsF contributed to mechanical reinforcement and swelling suppression. As the CsF content increased to 1.0 wt%, the dry tensile strength, Young's modulus, and toughness of the composite film increased to 75.7 MPa, 16.8 MPa, and 2.69 MJ m^{-3}, respectively. More importantly, the optimized film maintained a wet tensile strength of 4.3 MPa and a wet toughness of 1.12 MJ m^{-3} in the fully swollen state, while effectively suppressing excessive swelling. Furthermore, the degradation behavior of the PGM/CsF films could be regulated by CsF content, with complete degradation achieved within 60 days in natural soil and 90 days in enzyme-containing artificial seawater. Overall, this work demonstrates a feasible strategy for balancing wet mechanical robustness, transparency, and controllable degradability in PGA-based composite films, providing a promising route toward sustainable biodegradable film materials.

Author contributions

M. Wei, Y. Yao, and Y. Liu contributed equally to this work. Y.-I. Hsu, H. Uyama, W. Lu, and T. Chen conceived and designed the project. M. Wei, Y. Yao, and Y. Liu performed the experiments and investigation. X. Li and M. P. H. Pedige contributed to characterization, data analysis, and discussion. M. Wei, Y. Yao, and Y. Liu co-wrote the manuscript. Y.-I. Hsu, H. Uyama, W. Lu, and T. Chen supervised the project and contributed to the revision and editing of the manuscript.

Conflicts of interest

View Article Online
DOI: 10.1039/D6LP00162A

There are no conflicts to declare.

Acknowledgements

This work was supported by the National Natural Science Foundation of China (22322508) and the Natural Science Foundation of Ningbo (2024S069).

Notes and references

1 G. R. Mong, H. Tan, D. D. Chin Vui Sheng, H. Y. Kek, B. B. Nyakuma, K. S. Woon, M. H. D. Othman, H. S. Kang, P. S. Goh and K. Y. Wong, Journal of Cleaner Production, 2024, 434, 140180.
2 B. C. Gibb, Nat. Chem., 2019, 11, 394–395.
3 S. B. Borrelle, J. Ringma, K. L. Law, C. C. Monnahan, L. Lebreton, A. McGivern, E. Murphy, J. Jambeck, G. H. Leonard, M. A. Hilleary, M. Eriksen, H. P. Possingham, H. De Frond, L. R. Gerber, B. Polidoro, A. Tahir, M. Bernard, N. Mallos, M. Barnes and C. M. Rochman, Science, 2020, 369, 1515–1518.
4 F. De Marchis, T. Vanzolini, E. Maricchiolo, M. Bellucci, M. Menotta, T. Di Mambro, A. Aluigi, A. Zattoni, B. Roda, V. Marassi, R. Crinelli and A. Pompa, Biotechnology Journal, 2024, 19, 2300363.
5 D. Wu, J. Wang, Y. Zhao, S. Li, H. Yang, R. Tan and T. Zhang, Chemical Engineering Journal, 2024, 479, 147285.
6 X. Yue, H. Yang, Z. Han, Y. Lu, C. Yin, X. Zhao, Z. Liu, Q. Guan and S. Yu, Advanced Materials, 2024, 36, 2306451.
7 D. Li, Z. Han, Q. He, K. Yang, W. Sun, H. Liu, Y. Zhao, Z. Liu, C. Zong, H. Yang, Q. Guan and S. Yu, Advanced Materials, 2023, 35, 2208098.
8 T. Li, J. Kambanis, T. L. Sorenson, M. Sunde and Y. Shen, Biomacromolecules, 2024, 25, 5–23.
9 Y. Qiu, D. Zhang, Z. Zhou, D. Yang, C. Qian, C. Chen, Z. Zhao and H. Deng, Proc. Natl. Acad. Sci. U.S.A., 2025, 122, e2521173122.
10 Y. Chen, J.-Y. Han, G. Gao, J. Wang, W. Zhao, H. Yang, Y. Zhao, S. Wang and T. Zhang, Polymer, 2025, 331, 128506.
11 I. D. Haji Abdul Hamid, R. Soni, Y.-I. Hsu and H. Uyama, Polymer Degradation and Stability, 2024, 219, 110618.
12 K. Elbanna, F. S. Alsulami, L. A. Neyaz and H. H. Abulreesh, Front. Microbiol., 2024, 15, 1348411.
13 L. Wang, S. Chen and B. Yu, Trends in Food Science & Technology, 2022, 119, 1–12.
14 S.-B. Park, M.-H. Sung, H. Uyama and D. K. Han, Progress in Polymer Science, 2021, 113, 101341.
15 T. Castillo, C. Flores, H. Salgado-Lugo, C. F. Peña and E. Galindo, Electronic Journal of Biotechnology, 2023, 66, 38–51.
16 M. Wei, Y.-I. Hsu, T.-A. Asoh, M.-H. Sung and H. Uyama, J. Mater. Chem. B, 2021, 9, 3584–3594.
17 M. Karimi, F. T. Yazdi, S. A. Mortazavi, I. Shahabi-Ghahfarrokhi and J. Chamani, Polymer Testing, 2020, 83, 106338.
18 P. K. Panda, J.-M. Yang and Y.-H. Chang, International Journal of Biological Macromolecules, 2021, 171, 457–464.
19 K. Yu and M.-E. Aubin-Tam, ACS Appl. Nano Mater., 2020, 3, 12055–12063.
20 W. Pramualkijja and K. Srikulkit, ACS Omega, 2026, 11, 3839–3848.
21 Y. Yao, Y.-I. Hsu and H. Uyama, Polymer Degradation and Stability, 2025, 240, 111450.
22 H. Lee, K. Lee, M. Kim, Y. Kwon, J. Yun, J. H. Choi and H. J. Youn, Cellulose, 2025, 32, 4781–4796.

23 J. Zhang, L. Mao, S. Dai, H. Zhang, J. Xu, X. Liu, Q. Wei, M. Qin, C. Chen, Z. Gan and Z. Ning, Biomacromolecules, 2025, 26, 5927–5937.
24 Y. Hong, Y. Feng, H. Inuzuka and T. Aida, CCS Chem. 2025, 7, 2633–2642.
25 Y. Cheng, E. Hirano, H. Wang, M. Kuwayama, E. W. Meijer, H. Huang and T. Aida, Science, 2024, 386, 875–881.
26 G. Wang, D. Huang, J. Ji, C. Völker and F. R. Wurm, Advanced Science, 2021, 8, 2001121.
27 P. Wolf, M. Reimer, M. Maier and C. Zollfrank, Polymer Degradation and Stability, 2023, 217, 110538.
28 C.-C. Chen, L. Dai, L. Ma and R.-T. Guo, Nat Rev Chem, 2020, 4, 114–126.
29 Moataz. M. Nawar, E. Nassef, R. M. Thyab, T. M. Zewail, A. Abdelhafez and A. Morsy, *Polymer Engineering & Sci*, 2026, 66, 917–927.

View Article Online
DOI: 10.1039/D6LP00162A

View Article Online
DOI: 10.1039/D6LP00162A

Data Availability Statement

The data supporting this work are available within the article and its Supplementary Information.